ORIGINAL RESEARCH ARTICLE

Brivanib, a multitargeted small-molecule tyrosine kinase inhibitor, suppresses laser-induced CNV in a mouse model of neovascular AMD

Lele Li[1]* | Manhui Zhu[2]* | Wenli Wu[3] | Bai Qin[1] | Jiayi Gu[1] | Yuanyuan Tu[1] | Jianing Chen[3] | Dong Liu[4] | Yunwei Shi[4] | Xiaojuan Liu[5] | Aimin Sang[1]* | Dongmei Ding[6]*

[1]Department of Ophthalmology, Affiliated Hospital of Nantong University, Nantong, Jiangsu, China

[2]Department of Ophthalmology, Lixiang Eye Hospital of Soochow University, Suzhou, Jiangsu, China

[3]Medical College, Nantong University, Nantong, Jiangsu, China

[4]Co-innovation Center of Neuroregeneration, Jiangsu Key Laboratory of Neuroregeneration, Nantong University, Nantong, China

[5]Department of Pathogen Biology, Medical College, Nantong University, Nantong, Jiangsu, China

[6]Department of Ophthalmology, Laizhou City People's Hospital, Yantai, Shandong, China

Correspondence
Aimin Sang, Department of Ophthalmology, Affiliated Hospital of Nantong University, 226001 Nantong, China.
Email: sangam@ntu.edu.cn

Dongmei Ding, Department of Ophthalmology, Laizhou City People's Hospital, 264000 Yantai, China.
Email: dingdm2005@aliyun.com

Abstract

In age-related macular degeneration (AMD), choroidal neovascularization (CNV), a major pathologic feature of neovascular AMD (nAMD), affects 10% of patients, potentially causing serious complications, including vision loss. Vascular endothelial growth factor receptor 2 (VEGFR2) and fibroblast growth factor receptor 1 (FGFR1) contribute to the pathogenesis of CNV. Brivanib is an oral selective dual receptor tyrosine kinase (RTK) inhibitor of FGFRs and VEGFRs, especially VEGFR2 and FGFR1. In this study, brivanib inhibited zebrafish embryonic angiogenesis without impairing neurodevelopment. In a mouse CNV model, brivanib intravitreal injection blocked phosphorylation of FGFR1 and VEGFR2 and reduced CNV leakage, area, and formation without causing intraocular toxicity. Moreover, brivanib oral gavage reduced CNV leakage and area. Accordingly, brivanib remained at high concentrations (above 14,000 ng/ml) in retinal/choroidal/scleral tissues following intravitreal injection. Similarly, brivanib remained at high concentrations (over 10,000 ng/ml) in retinal/choroidal/scleral tissues following oral gavage. Finally, in vitro cell experiments demonstrated that brivanib inhibited the proliferation, migration and tube formation of microvascular endothelial cells. In conclusion, our study suggested that brivanib treatment could be a novel therapeutic strategy for nAMD.

KEYWORDS
age-related macular degeneration, choroidal neovascularization, fibroblast growth factor receptor 1, receptor tyrosine kinase inhibitor, vascular endothelial growth factor receptor 2

1 | INTRODUCTION

In age-related macular degeneration (AMD), choroidal neovascularization (CNV), a major pathologic characteristic of neovascular AMD (nAMD), occurs in 10% of patients (Dewan et al., 2006), potentially leading to serious complications, including fluid accumulation and subretinal hemorrhage with vision loss (Lim, Mitchell, Seddon, Holz, & Wong, 2012).

Although the pathogenesis of ocular neovascularization is undoubtedly complex, numerous experimental and clinical studies have revealed that vascular endothelial growth factor (VEGF) is a key mediator in the pathogenesis of intraocular disease with neovascularization (Aiello et al., 1995; Amadio, Govoni, & Pascale, 2016; Andreoli & Miller, 2007; Zhang, Han, Ru, Bo, & Wei, 2015). Currently, intravitreal injection of anti-VEGF is the first-line therapy for nAMD, which prevents abnormal angiogenesis and reduces exudation (Munk, Ruckert, Zinkernagel, Ebneter, & Wolf, 2016; Ng, Lai, Cheung, & Ohno-Matsui, 2017). However, the mechanisms upstream of VEGF secretion remain largely unclear. VEGF regulates endothelial cell (EC) function by binding to three vascular endothelial growth factor receptors (VEGFRs), including VEGFR1, VEGFR2, and VEGFR3. Among these receptors, VEGFR2, which is mainly expressed on ECs, mediates the proangiogenic effects of VEGF (Chiodelli et al., 2017). Fibroblast growth factor receptor 1 (FGFR1), belonging to the FGFR family of receptor tyrosine kinases (RTKs), conveys the signals of different fibroblast growth factors (FGFs) intracellularly (Sun et al., 2017). By activating multiple signaling cascades, including phospholipase C gamma (PLCγ) and signal transducer and activator of transcription (STAT), FGFs essentially control cell proliferation, survival, differentiation, and angiogenesis (Feng, Zhou, Nice, & Huang, 2015; Gouaze-Andersson et al., 2016). In particular, FGFR1 mRNA has been found to appear in the choroidal blood vessel walls of photocoagulation lesions in a mouse laser-induced CNV model (Matsushima et al., 1996). In addition, neovascularization after eye laser injury is obviously impaired in both Fgfr1/2 (Flk1-Cre) and Fgfr1/2 (Tie2-Cre) knockout mice, revealing a key requirement for autonomous EC FGFR signaling, particularly FGFR1 signaling, in laser-induced angiogenesis (Oladipupo et al., 2014).

Brivanib is an oral selective dual RTK inhibitor of FGFRs and VEGFRs, especially VEGFR2 and FGFR1 (Bhide et al., 2010), that has antitumor activity, including activity against persistent or recurrent cervical cancer and unresectable hepatocellular carcinoma (HCC; Chan et al., 2017; Sun & Cabrera, 2018), due to its strong antiangiogenic effects and potent direct effects. The activity of brivanib against both the VEGF and FGF pathways has aroused interest, as upregulation of proangiogenic pathways such as the FGF pathway facilitates the development of resistance to anti-VEGF therapies (Bergers & Hanahan, 2008). Thus, we wondered whether brivanib could alleviate CNV formation via inhibition of the VEGFR2 and FGFR1 pathways.

In the present study, wild-type (WT) and transgenic zebrafish lines and a mouse laser-induced CNV model were used to investigate the effects and underlying mechanisms of brivanib during nAMD pathogenesis. Brivanib inhibited zebrafish embryonic angiogenesis without impairing neurodevelopment. In the mouse CNV model, brivanib intravitreal injection blocked the phosphorylation of FGFR1 and VEGFR2 and reduced CNV leakage, area and formation without causing intraocular toxicity. Moreover, brivanib oral gavage reduced CNV leakage and area. Accordingly, brivanib remained at high concentrations (above 14,000 ng/ml) in retinal/choroidal/scleral tissues following intravitreal injection. Similarly, brivanib remained at high concentrations (10,000 ng/ml) in retinal/choroidal/scleral tissues following oral gavage. Finally, in vitro cell experiments demonstrated that brivanib inhibited the proliferation, migration, and tube formation of microvascular endothelial cells (VECs). These results could be helpful in understanding the effects and mechanisms of brivanib in CNV and determining potential novel therapeutic strategies for nAMD patients.

2 | MATERIALS AND METHODS

2.1 | Zebrafish and drug treatment

This study was conducted in accordance with the Local Institutional and Chinese Laws for the Protection of Animals. Zebrafish embryos were obtained through natural mating. The embryos were raised and maintained under standard conditions at the Zebrafish Center of Nantong University. The transgenic zebrafish lines Tg(Flk: mCherry::Hb9:EGFP), which expressed mCherry (red) under the control of Flk (also named vascular endothelial growth factor receptor 2, a vascular endothelial cell marker) and enhanced green fluorescent protein (EGFP) (green) under the control of Hb9 (also named motor neuron and pancreas homeobox 1, a differentiated motor neuron marker); Tg(Flk:mcherry::Fli:nGFP), which expressed mCherry (red) under the control of Flk and nGFP (green) under the control of Fli (an EC marker) to label the nuclei of ECs; and Tg (Flk:EGFP), which expressed EGFP (green) under the control of Flk, were used. At 6 hr post fertilization (hpf), the zebrafish embryos were examined under anatomical microscopy, and abnormal individuals were excluded. Approximately 10 healthy embryos were placed into each well of a 96-well plate with E3 solution. At 8 hpf, the E3 solution in each well was replaced with a treatment solution containing brivanib (BMS-540215; Selleck) at a concentration of 0.0005, 0.001, 0.01, 0.1, 1, 5, 10, 50, 100 or 200 μg/ml. At 48 hpf, the zebrafish embryos were collected for imaging and fixed with 4% paraformaldehyde (PFA) in phosphate-buffered saline (PBS) for staining of ISVs, neurons, EC nuclei, brain tissue, and eye vessels.

2.2 | Imaging

At 48 hpf, embryos for confocal imaging were anesthetized with E3/0.16 mg/ml tricaine/1% 1-phenyl-2-thiourea (Sigma) and embedded in 0.8% low-melting-point agarose. Images were acquired with a confocal microscope (Leica TCS-SP5 LSM; Leica Microsystems GmbH, Germany).

2.3 | Mouse laser-induced CNV model

Nine to 10 weeks old male C57BL/6 mice were maintained and bred at the Experimental Animal Center, Nantong University (Jiangsu, China). Approval was obtained from the Animal Research Ethics Committee, Nantong University, in agreement with the Chinese National Standard. Anesthesia was induced by intraperitoneal injection of pentobarbital (0.05 mg/g body weight), and the pupils of the mice were dilated with topical 5% tropicamide (Santen, Japan). Following mydriasis, the mice were placed on a platform under a slit lamp, and the corneas were anesthetized with 0.5% proparacaine hydrochloride eye drops (Alcon Laboratories). Laser photocoagulation (659 nm laser, 250 mW, 50 ms duration, 50 μm spot) was performed bilaterally in each mouse. Only burns in which a bubble was produced were included in our study. Spots containing hemorrhage or failing to develop a bubble at the laser site were excluded. The eyes were subsequently coated with erythromycin eye ointment. The sham-treated mice were appointed as the normal (N) control group.

2.4 | Western blot analysis

Protein extracts were obtained from retinal/choroidal/scleral tissues homogenized using a Tissue Lyser II (Qiagen, Germany) in different groups, and the protein concentrations were determined using a Bradford assay. Approximately 5 mg of total protein per sample was diluted with sample buffer with 20% 2-mercaptoethanol (Wako). After heating at 70°C for 10 min, the samples were subjected to 10% SDS-PAGE (Wako). The separated proteins were electroblotted onto a polyvinylidene fluoride (PVDF) membrane (Millipore). The membrane was blocked with 50 mg/ml skim milk (Guangming, China) in PBS for 1 hr at room temperature. Anti-p-FGFR1 (ab173305; phospho Y653; Abcam), anti-FGFR1 (60325-1-Ig; Proteintech), anti-p-VEGFR2 (ab5473; phospho Y1054 plus Y1059; Abcam), anti-VEGFR2 (26415-1-AP; Proteintech), and anti-GAPDH (sc-365062; Santa Cruz) antibodies were used and blotted with goat anti-rabbit (ab6721; Abcam) and goat anti-mouse HRP-conjugated secondary antibodies (ab6789; Abcam). The immunoreactive proteins were detected with an ECL Chemiluminescence System (Beyotime Institute of Biotechnology) and were imaged with a Chemiluminescence Gel Imager (Bio-Rad). The band intensities were measured with ImageJ software (http://rsb.info.nih.gov/ij).

2.5 | Immunohistochemistry of choroidal flat mounts

On Day 7 or Day 14 after laser treatment, the cornea and crystalline lens were removed from each enucleated eye, and then a radial relaxing incision was made in the eyecup of the choroid and sclera. The tissues were then fixed with 4% PFA for 20 min, and the retina and sclera were removed from the choroid. The choroidal flat mounts were stained for IB4 and p-FGFR1, p-VEGFR2, CD31, or phalloidin. The flat mounts were incubated with a 1 mg/ml solution of Alexa Fluor 488-conjugated isolectin-B4 (IB4; I21411) and Alexa Fluor 568-conjugated phalloidin (A12380) antibodies prepared in ICC buffer (1 × PBS, 0.5% bovine serum albumin (BSA), 0.2% Tween 20, 0.05% sodium azide, pH 7.3) at 4°C for 24 hr. Both antibodies were obtained from Thermo Fisher Scientific, Waltham, MA. The other antibodies included anti-p-FGFR1 (ab173305), anti-p-VEGFR2 (ab5473), and anti-CD31 (ab28364) primary antibodies and an Alexa Fluor 568-conjugated goat anti-rabbit IgG (H+L) secondary antibody (A-11036; Thermo Fisher Scientific). The slides were also stained with 4′,6-diamidino-2-phenylindole (DAPI; D9542; Sigma) and mounted (Aqua-Poly/Mount; 18606-100; Polysciences). Photomicrographs were captured with a confocal microscope (Leica TCS-SP5 LSM; Leica Microsystems GmbH). The IB4-positive CNV areas were quantified with ImageJ software. Lesions with obvious hemorrhaging or bridging CNV were excluded. The images were measured by two researchers in a masked procedure.

2.6 | Intravitreal injection

Intravitreal injection into the right eyes of mice was performed 3 days after laser treatment. First, the mice were anesthetized by intraperitoneal injection of 1% mebumal sodium, and the pupils were dilated. Both eyes were covered with sodium hyaluronate. Next, an aperture 1 mm posterior to the superotemporal limbus was made with a 30-gauge needle. A blunt 33-gauge needle was inserted through the opening, and 1 μl of brivanib solution (5 μg/μl in 0.1% dimethyl sulfoxide [DMSO]); 1 μl of a solution of ranibizumab (RBZ), which is a recombinant humanized monoclonal antibody fragment binding all active isoforms of VEGF-A (RBZ; Lucentis; Genentech Inc.; 10 μg/μl in 0.1% DMSO, used as the positive control); or an equivalent volume of 0.1% DMSO was injected slowly over 30 s to permit diffusion of the liquid. Subsequent fundus evaluation demonstrated no adverse effects from the intravitreal injection. Tobramycin eye drops were topically administered to the treated eyes three times per day in the week following intravitreal injection. Individuals with retinal bleeding after injection were excluded.

2.7 | Fundus fluorescein angiography

Fundus fluorescein angiography (FFA) was performed to analyze leakage with a retinal imaging microscope (Micron IV; Phoenix Research Laboratories) 7 days or 14 days after laser photocoagulation. Mice were anesthetized and their pupils dilated; the mice were then intraperitoneally injected with AK-Fluor fluorescein (Akorn) at 5 μg/g body weight. Fluorescent fundus images were taken with a retinal imaging microscope at 5 and 10 min after fluorescein injection. The difference in integrated intensity between 5 and 10 min was recorded as an indicator of vascular leakage. The fluorescent intensity of CNV lesions was graded using ImageJ by two masked researchers using the following criteria: 0 (not leaky), faint hyperfluorescence or mottled fluorescence without leakage; 1 (questionable leakage), hyperfluorescence of lesions without progressive increases in size or intensity; 2A (leaky), hyperfluorescence increasing in intensity but not in size; and 2B (pathologically significant leakage), hyperfluorescence increasing in both intensity and size (Yu et al., 2008).

2.8 | Indocyanine green angiography

Mice were anesthetized, and their pupils were dilated. The mice were then intraperitoneally injected with indocyanine green (ICG; 6 mg/kg body weight; Sigma). The eyes were dilated with 1% tropicamide to obtain ICG angiography images. All images were taken with a Heidelberg Spectralis (Heidelberg Engineering, Germany).

2.9 | Hematoxylin–eosin staining of paraffin sections

After each animal was killed by cervical dislocation, the eyeballs were enucleated, fixed in 4% PFA, conventionally dehydrated and embedded in paraffin wax. The optic nerve parallel to the sagittal plane at the laser photocoagulation position was selected, and slices with a thickness of 6.0 μm were prepared continuously. The sections were stained with Hematoxylin–eosin (HE) and observed and photographed under a light microscope (Leica DM1000). The ratio of A (the distance from the ganglion cell layer to the outer edge of the inner nuclear layer) to B (the distance from the ganglion cell layer to the outer edge of the outer nuclear layer) was calculated with ImageJ.

2.10 | TUNEL assay

A TUNEL assay was performed on 8 mm cryosections of mouse eyes. The slides were dried at room temperature for 30 min. The tissue was permeabilized with 0.1% Triton X-100% and 0.1% sodium citrate for 2 min on ice. TUNEL labeling was performed with an In Situ Cell Death Detection Kit with TMR red (Roche, Germany). The sections were incubated and covered with parafilm for 60 min at 37°C. Then, the sections were counterstained with DAPI. Coverslips were mounted. TUNEL and DAPI staining were visualized with a confocal microscope (Zeiss 510 META confocal microscope; Carl Zeiss MicroImaging).

2.11 | Oral gavage of brivanib

On Day 0, laser photocoagulation was performed on mice. Mice without laser treatment were taken as the normal group. From Day 3 to Day 7, laser-treated mice were randomly chosen to receive 100 or 200 mg/kg/day brivanib via an oral gavage needle daily in addition to an ordinary mouse diet (to form the 100 and 200 mg/kg/day brivanib groups). On Day 14, all mice were killed. Laser-treated mice receiving only an ordinary diet were taken as the CNV Day 14 group.

2.12 | Analysis of brivanib concentrations in mouse plasma and retinal/choroidal/scleral tissues

The brivanib concentrations in mouse plasma and retinal/choroidal/scleral tissues following brivanib intravitreal injection or oral gavage was measured at 0, 4, 8, 12, 16, 20 24, 28, 32, 36, 40, 44, and 48 hr through solid-phase extraction followed by liquid chromatography/tandem mass spectrometry using a stable-labeled internal brivanib standard ([$^{13}C_3$, $^{15}N_2$] BMS-540215). The internal standard (50 μl at 100 ng/ml) was added to 0.1 ml of sample. The plasma samples were buffered with ammonium formate before being loaded onto a solid-phase extraction plate obtained from Waters (Milford, MA). The solid-phase extraction plates were conditioned with methanol and an ammonium formate solution. After addition of RPE/choroidal tissues, the cartridges were washed with an ammonium formate solution and an acetonitrile/water solution. The tissues were eluted from the plate with a formic acid solution, evaporated to dryness under nitrogen, and then reconstituted with an acetonitrile/water/ammonium formate/formic acid solution. The urine samples were buffered with ammonium formate followed by acetonitrile, vortexed, and then centrifuged; these extracts were loaded into a high-performance liquid chromatography (HPLC) system. The HPLC system contained a Shimadzu HPLC pump (Shimadzu Corporation, Columbia, MD) and a PerkinElmer Autosampler (PerkinElmer Life Sciences, Inc., Boston, MA). The column used was a Gemini C6-phenyl column (5 μm, 2.0 × 50 mm; Phenomenex, Torrance, CA), and the mobile phase flow rate was 0.3 ml/min. A gradient of two solvent systems, A and B, was used for HPLC profiling. Solvent A was a 0.01 M ammonium formate solution. Solvent B consisted of 0.01 M ammonium formate with 0.12% formic acid in acetonitrile/water. The HPLC system was interfaced to a Sciex API 4000 mass spectrometer (Applied Biosystems, Foster City, CA) that was operated in the positive-ion electrospray ionization mode. The analysis times were 2.3 and 3.5 min for both brivanib and the internal standard in the plasma and retinal/choroidal/scleral tissues, respectively. The limits of quantitation were 1–10,000 ng/ml and 2–20,000 ng/ml in the plasma and retinal/choroidal/scleral tissues, respectively.

2.13 | Cell culture and treatment

The murine brain microvascular endothelial cell line b-End3 was obtained from the American Type Culture Collection (ATCC CRL-2299, Manassas, VA). b-End3 cells were constructed from brain ECs of 129/Sv mice by immortalization via the polyomavirus middle T-antigen (Williams et al., 1989). The cells were maintained in Dulbecco's modified Eagle's medium (DMEM; Gibco, Thermo Fisher Scientific) containing 1 g/l glucose supplemented with 10% fetal bovine serum (FBS; Gibco), 1% nonessential amino acids, 100 IU/ml penicillin, and 100 μg/ml streptomycin (Gibco) at 37°C with 5% CO_2. The b-End3 cells were treated with dimethyloxalylglycine (DMOG; Sigma) diluted in 0.5% (volume/volume; v/v) DMSO (diluted in 1 × PBS) to a concentration of 0.4 mM (the hypoxia group) or with the same volume of 0.5% DMSO (the DMSO group) for 6 hr. The cells in the brivanib group were treated with 10 mM brivanib for 6 hr (at the same time as DMOG treatment).

2.14 | 5-Ethynyl-20-deoxyuridine assay

An EdU Kit (Cell Light EdU DNA Imaging Kit, RiboBio) was used to evaluate b-End3 cell proliferation ability according to the manufacturer's instructions. Images were obtained and analyzed with a

microscope (Olympus, Tokyo, Japan). The ratio of 5-ethynyl-20-deoxyuridine (EdU)-stained cells (red fluorescence) to DAPI-stained cells (blue fluorescence) was used to evaluate cell proliferation activity.

2.15 | Transwell migration assay

B-End3 cells (2.5×10^5) were suspended in 250 μl of serum-free DMEM and seeded in the top chambers of 24-well Transwell plates (Corning Inc., Corning, NY). The bottom chambers of the Transwell plates were filled with 600 μl of DMEM containing 10% FBS. After 48 hr, the bottom of each chamber insert was stained with methanol and 0.1% crystal violet, and the cells were imaged and counted using an Olympus IX70 inverted microscope (Tokyo, Japan). The ImageJ software (NIH, Bethesda, MD) was used to obtain an average cell count of four stained membrane images. Each assay was repeated in triplicate.

2.16 | Tube formation assay

The angiogenic ability of b-End3 cells was assessed with an in vitro Matrigel-based tube formation assay. Briefly, 50 μl of Matrigel Basement Membrane Matrix was coated onto a 96-well plate, and the plate was incubated at 37°C for 30 min. B-End3 cells (3×10^4) were seeded on the Matrigel and treated as indicated for a total of 6 hr. Images were acquired of five randomly chosen microscopic fields. The cumulative tube length was analyzed with an IX70 microscope at ×200 magnification.

2.17 | Statistical analysis

The data are presented as the mean ± standard error of the mean and were analyzed with Dunnett's or Tukey's multiple comparison tests. A *p* value of <.05 was considered to indicate statistical significance.

3 | RESULTS

3.1 | Brivanib blocks zebrafish embryonic angiogenesis without neurodevelopment impairment

To identify a suitable dose of brivanib, we treated WT zebrafish embryos in triplicate with 0.0005, 0.001, 0.01, 0.1, 1, 5, 10, 50, 100 or 200 μg/ml brivanib solution from 8–48 hpf (Figure 1a). Brivanib treatment at concentrations beyond 10 μg/ml caused embryos to die (Figure 1b). Brivanib treatment at a concentration of 200 μg/ml resulted in the death of almost all embryos (Figure 1b). Some of the embryos treated with brivanib below 5 μg/ml appeared normal (Figure 1b). Because brivanib treatment beyond 1 μg/ml caused an extremely severe phenotype, we selected 0.001, 0.01, 0.1, and 1 μg/ml as the working concentrations in the subsequent experiments.

To verify the effects of brivanib on zebrafish embryonic angiogenesis and neurodevelopment, we used the transgenic line Tg(Flk:mcherry::Hb9:EGFP), in which VECs and motor neurons are labeled with mCherry and EGFP, respectively. Each concentration of brivanib significantly inhibited ISV branching angiogenesis (Figure 1c, upper line) without affecting neuronal development (Figure 1C, middle line). Similarly, in the line Tg(Flk:mcherry::Fli:nGFP), brivanib treatment dramatically inhibited ISV branching angiogenesis (Figure 1d, upper line) and decreased the number of ECs (Figure 1d, middle line). In particular, in the line, Tg(Flk:EGFP), in which VECs are labeled with EGFP, zebrafish embryonic brain, and eye vessels were hampered by brivanib treatment (Figure 1e). The data suggested that brivanib inhibited the angiogenesis of zebrafish embryos without affecting their neurodevelopment.

3.2 | Phosphorylation of the brivanib target molecules FGFR1 and VEGFR2 is increased in the mouse CNV region

Brivanib is a receptor tyrosine kinase inhibitor (TKI) with a broad range of targets, including FGFR1 and VEGFR2 (Ayers, Fargnoli, Lewin, Wu, & Platero, 2007). Therefore, we used laser photocoagulation to construct a mouse CNV model and found that p-FGFR1 and p-VEGFR2 increased following laser exposure, peaking at Day 7 (Figure 2a,b). Immunofluorescence staining also showed that p-FGFR1 and p-VEGFR2 were increased at Day 7 following laser injury and that they were colocalized with IB4 (a vascular endothelial cell marker; Figure 2c,d). The results suggested that phosphorylation of the brivanib target molecules FGFR1 and VEGFR2 is increased in the mouse CNV region.

3.3 | Brivanib intravitreal injection inhibits the phosphorylation of FGFR1 and VEGFR2 and reduces CNV leakage and area

To identify the effects and mechanisms of brivanib in CNV, brivanib intravitreal injection was performed 3 days following laser injury, and analysis was performed at Day 7 (Figure 3a). Brivanib, but not RBZ, downregulated p-FGFR1 and p-VEGFR2 levels in CNV mice, as measured after Day 7 (Figure 3b,c). The concentration–time profiles of brivanib in the retinal/choroidal/scleral tissues from mice following brivanib intravitreal injection showed that brivanib reached its peak concentrations at 4 hr (15623.89 ng/ml ± 456.77 ng/ml) and that high concentrations were sustained until 20 hr (Figure 3d). FFA showed that CNV leakage was decreased in the brivanib and RBZ groups compared to the control groups (Figure 3e). The leakage score analysis further showed that the percentages of 0 and 1 scores were increased in the brivanib and RBZ groups compared to the control groups, while the percentages of 2A and 2B scores were decreased (Figure 3g). Additionally, the mean intensity values showed that CNV leakage was decreased in the brivanib and RBZ groups (Figure 3h). Indocyanine green angiography (ICGA) showed that the CNV area was also decreased in the brivanib and RBZ groups (Figure 3f). The results suggested that brivanib intravitreal injection reduced CNV leakage and area, possibly by inhibiting the phosphorylation of FGFR1 and VEGFR2.
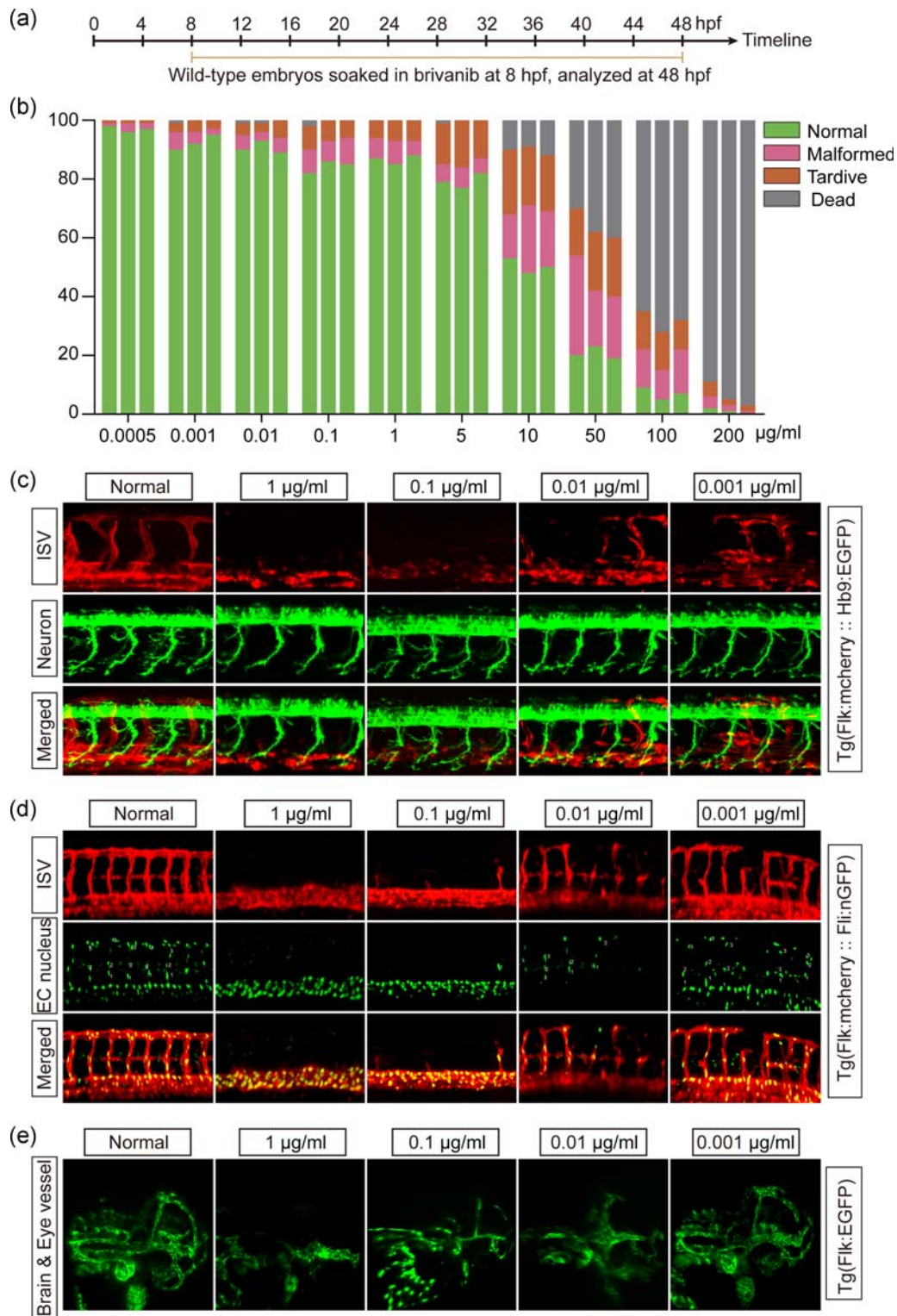
FIGURE 1 Brivanib hinders zebrafish embryonic angiogenesis without causing neurodevelopment impairment. (a) The timeline shows that wild-type zebrafish embryos were soaked in brivanib (0.0005, 0.001, 0.01, 0.1, 1, 5, 10, 50, 100 or 200 μg/ml) at 8 hpf and analyzed at 48 hpf. (b) The percentages of embryos of different phenotype induced by different concentrations of brivanib treatment at 8 hpf and analyzed at 48 hpf. The experiments with brivanib treatment were repeated in triplicate for each concentration. The percentages of normal, malformed, tardive, and dead embryos are shown in the green, pink, orange, and gray columns, respectively. (c) The mCherry-positive (red) intersegmental vessel (ISV) phenotypes and the EGFP-positive (green) cells in neural tubes of the normal and 0.001, 0.01, 0.1, and 1 μg/ml brivanib-treated groups. Merged images of ISVs and neural tubes are shown in the bottom row. (d) The mCherry-positive (red) ISV phenotypes and nGFP-positive (green) endothelial cell (EC) nuclei of the normal and 0.001, 0.01, 0.1, and 1 μg/ml brivanib-treated groups. (e) EGFP-positive (green) brains and eye vessels of the normal and 0.001, 0.01, 0.1, and 1 μg/ml brivanib-treated groups. Scale bar = 100 μm in Labels c, d, and e. n = 8/group. EGFP: enhanced green fluorescent protein; ISV: intersegmental vessel [Color figure can be viewed at wileyonlinelibrary.com]
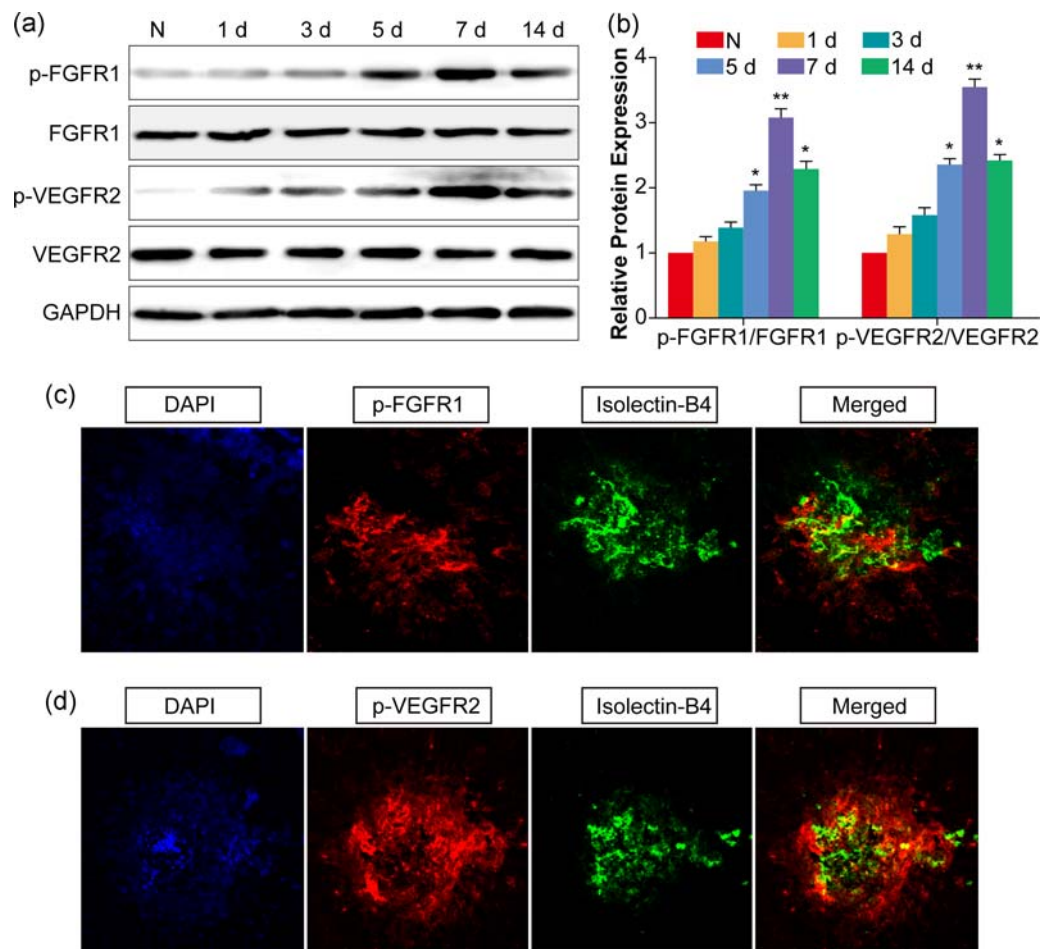
FIGURE 2 Phosphorylation of the brivanib target molecules FGFR1 and VEGFR2 is increased in the mouse CNV region. A mouse CNV model was constructed by laser photocoagulation. (a) The p-FGFR1, FGFR1, p-VEGFR2, and VEGFR2 protein levels were detected by Western blot analysis in the normal and CNV Day 1, 3, 5, 7, and 14 groups. (b) Quantification of the p-FGFR1 and p-VEGFR2 protein levels in each group. $n = 6$/group, $**p < .01$ versus the normal group. (c) Choroidal flat mounts from the CNV Day 7 group were stained with DAPI (nuclei), anti-p-FGFR1, and fluorescent anti-isolectin B4 (IB4) antibodies. (d) Choroidal flat mounts from the CNV Day 7 group were stained with DAPI (nuclei), anti-p-VEGFR2, and anti-IB4 antibodies. Scale bar = 100 μm. $n = 8$/group. CNV: choroidal neovascularization; DAPI: 4′,6-diamidino-2-phenylindole; FGFR1: fibroblast growth factor receptor 1; VEGFR2: vascular endothelial growth factor receptor 2 [Color figure can be viewed at wileyonlinelibrary.com]

3.4 | Brivanib intravitreal injection ameliorates CNV formation without causing intraocular toxicity

To further explore the therapeutic and potential adverse effects of brivanib in the context of CNV in mice, staining of IB4 and CD31 (an EC marker) was performed on choroidal flat mounts, and the results showed that brivanib alleviated CNV formation (Figure 4a,d). In wild-type zebrafish embryos, brivanib treatment beyond 10 μg/ml caused some embryos to die (Figure 1b). The question of whether brivanib could cause mouse eye cell apoptosis was answered by the results that eye cell apoptosis was unaffected in the brivanib group compared to the normal and CNV Day 7 groups (Figure 4b). Examination of HE-stained retinal sections (Figure 4c) and quantification of retinal thickness (Figure 4e) revealed no differences in histologic morphology or retinal thickness between normal and brivanib-treated eyes. These data suggested that brivanib alleviated mouse CNV formation without causing intraocular toxicity.

3.5 | Brivanib oral gavage reduces CNV leakage and area

To further confirm the effect of brivanib on the pathogenesis of CNV, brivanib was given by oral gavage at a dose of 100 or 200 mg/kg/day from Day 3 until Day 7 after laser injury, and analysis was performed on Day 14 (Figure 5a). FFA showed that CNV leakage was decreased in the brivanib groups compared to the control group (Figure 5b). The leakage score analysis also showed that the percentages of 0 and 1 scores were increased in the brivanib groups, while the percentages of 2A and 2B scores were decreased (Figure 5e). The FFA results and mean intensity values showed that CNV leakage was decreased in the brivanib groups (Figure 5b,f). ICGA showed that the CNV area was decreased in the brivanib groups (Figure 5c). Furthermore, phalloidin (an F-actin marker) and IB4 staining also showed that brivanib decreased the CNV area (Figure 5d,g). The data suggested that brivanib oral gavage also reduced CNV leakage and area.
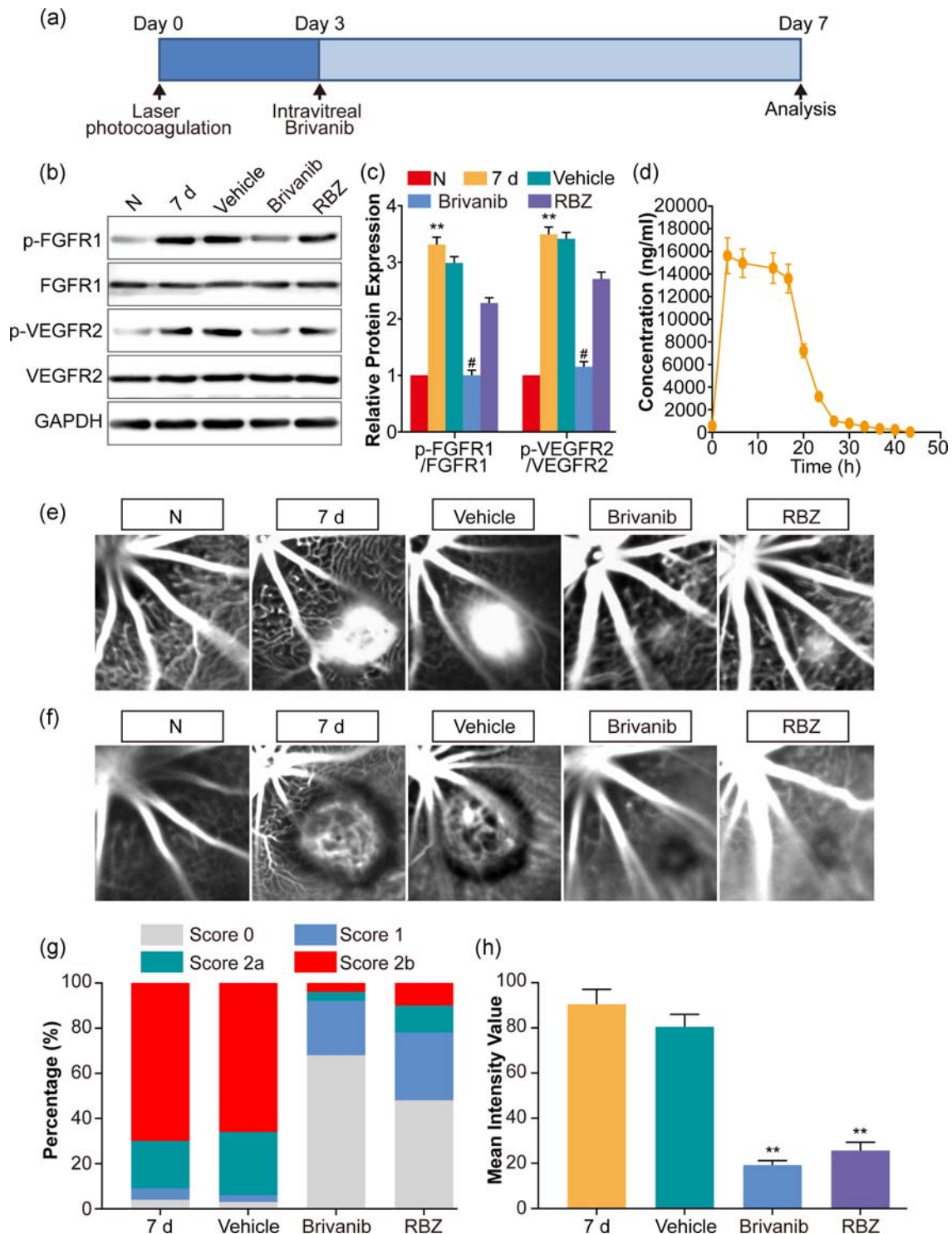
FIGURE 3 Brivanib intravitreal injection downregulates the phosphorylation of FGFR1 and VEGFR2 and reduces CNV leakage and area. (a) Schematic diagram of the experimental procedure. The mice (Day 7 group) were treated with a laser on Day 0. On Day 3, 1 μl of 0.1% DMSO (vehicle group), 2 μg/μl brivanib (brivanib group) or 10 μg/μl RBZ (RBZ group) was injected intravitreally. The mouse eye tissues were collected and analyzed on Day 7. (b) The protein levels of p-FGFR1, FGFR1, p-VEGFR2, and VEGFR2 in the normal, Day 7, vehicle, brivanib, and RBZ groups were detected by Western blot analysis analysis. (c) Quantification of the p-FGFR1 and p-VEGFR2 protein levels in each group. $n = 6$/group, *$p < .05$, **$p < .01$ versus the normal group. (d) Mean retinal/choroidal/scleral concentration–time profiles of brivanib in mice after intravitreal injection of [^{14}C] brivanib alaninate. (e) FFA and (f) ICGA were performed in each group. $n = 5$ in each group. (g) FFA was performed on CNV lesions, and fluorescein leakage in CNV lesions was graded for the Day 7 ($n = 31$ lesions), vehicle ($n = 29$ lesions), brivanib ($n = 31$ lesions), and RBZ ($n = 30$ lesions) groups. Scale bar = 200 μm. (h) The mean intensity values representing CNV leakage were assessed by FFA and quantified. **$p < .01$ versus the Day 7 group. CNV: choroidal neovascularization; DMSO: dimethyl sulfoxide; FFA: fundus fluorescein angiography; ICGA: indocyanine green angiography; RBZ: Ranibizumab; VEGFR2: vascular endothelial growth factor receptor 2 [Color figure can be viewed at wileyonlinelibrary.com]
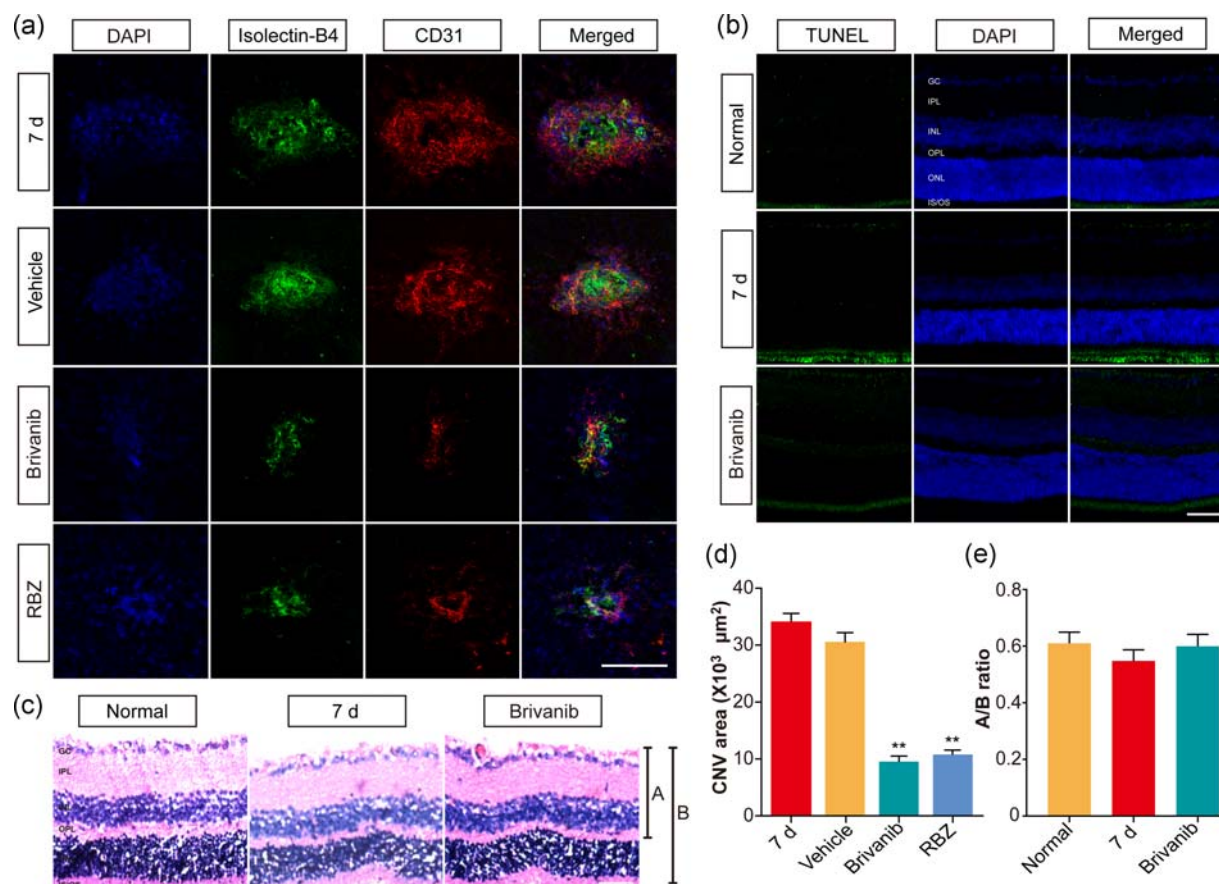
FIGURE 4 Brivanib alleviates CNV formation without inducing intraocular toxicity. (a) Mouse choroid flat mounts from the CNV Day 7, CNV Day 7 plus vehicle, CNV Day 7 plus brivanib, and CNV Day 7 plus RBZ groups were stained with DAPI (blue), anti-IB4 (green), and anti-CD31 (red) antibodies. (b) TUNEL (green) and DAPI (blue) immunofluorescence staining of mouse choroid/RPE/retina cryosections from the normal, CNV Day 7, and CNV Day 7 plus brivanib groups (GC: ganglion cell layer; INL: inner nuclear layer; IPL: inner plexiform layer; IS: inner segment; ONL: outer nuclear layer; OPL: outer plexiform layer; OS: outer segment). (c) Mouse choroid/RPE/retina complexes were stained with HE in the normal, CNV Day 7, and CNV Day 7 plus brivanib groups. Scale bar = 100 μm in (a). Scale bar = 50 μm in b,c. n = 8/group. (d) Quantification of the CNV area. $**p < 0.01$ versus CNV Day 7 group. (E) Quantification of the ratio of A to B displayed in (c). CNV: choroidal neovascularization; DAPI: 4′,6-diamidino-2-phenylindole [Color figure can be viewed at wileyonlinelibrary.com]

Additionally, the concentration-time profiles of brivanib in plasma showed that brivanib concentrations increased from 4 hr, reached a peak at 12 hr (9862.78 ng/ml ± 671.43 ng/ml) and remained high until 16 hr (Figure 5h). Similarly, the concentration–time profiles of brivanib in retinal/choroidal/scleral tissues from mice following brivanib oral gavage showed that brivanib concentrations increased quickly from 4 hr, peaking at 12 hr (13235.67 ng/ml ± 863.54 ng/ml), and remained high until 16 hr (Figure 5i).

3.6 | Brivanib inhibits the proliferation, migration, and tube formation of b-End3 cells in vitro

To further identify the antiangiogenic effect of brivanib on choroid microvascular endothelial cells, the mouse brain microvascular endothelial cell line b-End3 was exposed to hypoxia and brivanib to mimic brivanib therapy in the context of mouse CNV (Izumi-Nagai et al., 2008). The results showed that brivanib decreased the proportion of EdU-positive cells (Figure 6a,d), the number of migrated cells, (Figure 6b, e), and the number of closed tubes in the brivanib+hypoxia group compared

to the hypoxia-only group (Figure 6c,f) suggesting that brivanib inhibited the proliferation, migration, and tube formation of b-End3 cells in vitro.

4 | DISCUSSION

Brivanib is a dual TKI of VEGFR1–3 and FGFR1–3 that is used in patients resistant to anti-VEGF therapy (Kudo et al., 2014). Brivanib has been used for clinical therapy or in trials for various cancers, including advanced HCC, advanced/metastatic colorectal cancer, and endometrial cancer (Ba-Sang et al., 2016; Cucchetti et al., 2017; Papa et al., 2016). In the present study, brivanib inhibited zebrafish embryonic angiogenesis without causing neurodevelopment impairment in the zebrafish trans-genic line Tg(Flk:mcherry::Hb9:EGFP; Figure 1c). Moreover, in a mouse laser-induced CNV model, brivanib alleviated CNV formation without causing intraocular toxicity, as verified by an apoptosis assay (Figure 4b), HE staining (Figure 4c), and quantitative analysis (Figure 4e). All of these data indicate the advantages of brivanib for therapeutic use. However, in clinical trials, brivanib is less well tolerated than sorafenib. In one study,

treatment was discontinued due to side effects in 43% of the brivanib group compared to 33% of the sorafenib group (Johnson et al., 2013). The main grade 3/4-related side effects are diarrhea (4%) and hypertension (26%; Diaz-Padilla & Siu, 2011). Thus, the side effects of brivanib used in nAMD patients need further investigation.

Brivanib is a small molecular inhibitor of the VEGFR and FGFR signaling pathways. In our study, only VEGFR2 and FGFR1 were analyzed, and the results indicated that p-VEGFR2 and p-FGFR1 were increased in the mouse laser-induced CNV model (Figure 2a,b). Additionally, brivanib intravitreal injection inhibited the
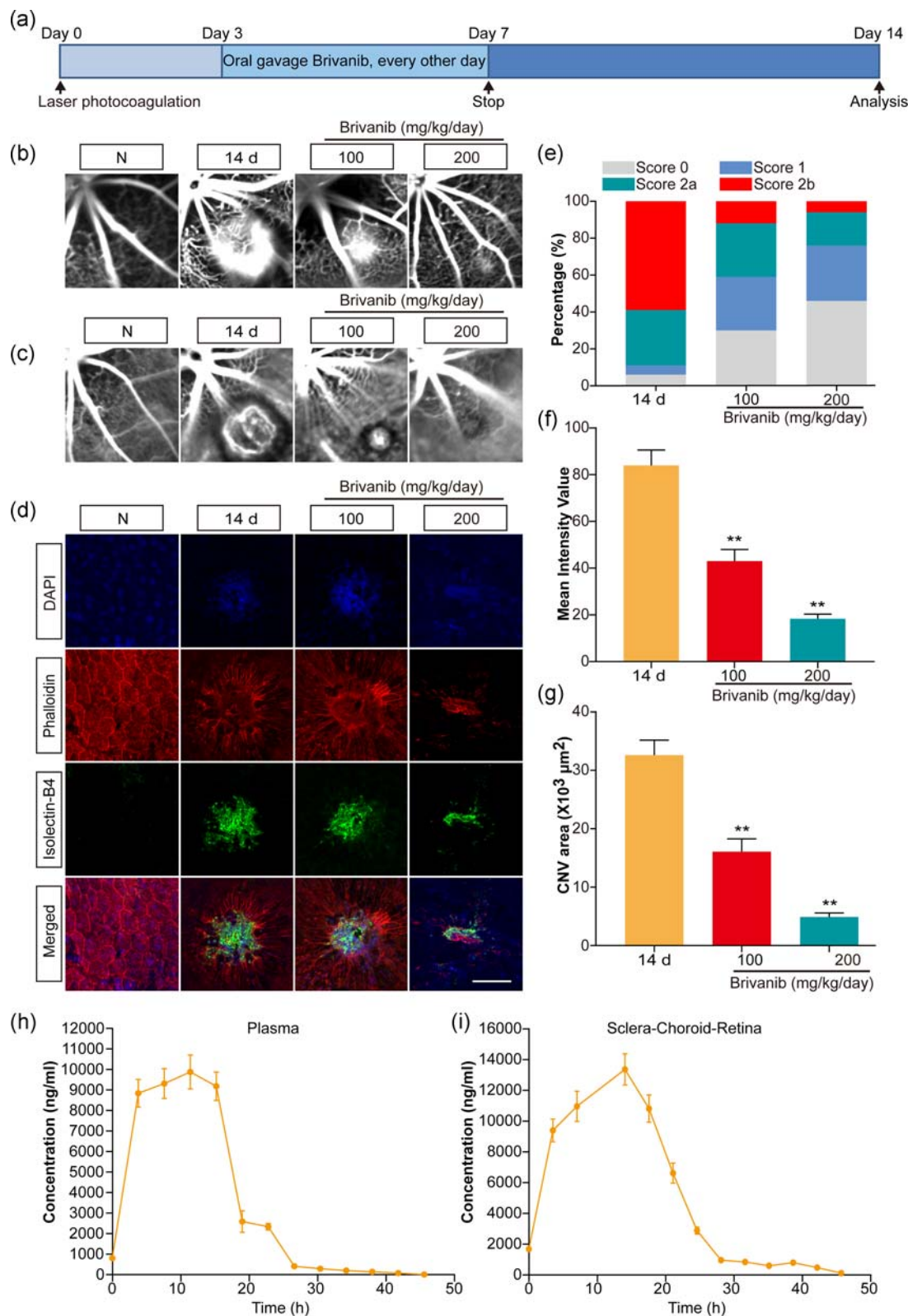

FIGURE 5 Continued.

phosphorylation of VEGFR2 and FGFR1 (Figure 3b,c). Vascular endothelial growth factor receptor 1 (VEGFR1, also known as FLT1) regulates the recruitment and infiltration of proinflammatory cells into pathological sites under different disease conditions. For example, in mouse laser-induced CNV, deficiency of placental growth factor (PlGF), a ligand for VEGFR1, significantly inhibits infiltration of macrophages/microglia (F4/80-positive cells) into CNV lesions (Van de Veire et al., 2010). Moreover, anti-PlGF treatments decrease overall numbers of activated subretinal mononuclear phagocytes, especially cells expressing PlGF, in mouse laser-induced CNV (Crespo-Garcia et al., 2017). In Alzheimer's disease, VEGFR1 acts as an integral chemotactic component in attracting microglia into neurodegenerative areas due to an amyloid-β peptide (Ryu, Cho, Choi, Wang, & McLarnon, 2009). FGF directly participates in the genesis of blood capillaries and lymphatic vessels (Cao et al., 2012). Furthermore, FGF2 acts as a direct activator of phosphatidylinositol-4,5-bisphosphate 3-kinase (PI3K) and protein kinase B (Akt), which are key stimuli initiating EC migration, invasion, and differentiation (Yu et al., 2018; Zubilewicz et al., 2001). Following FGF2 binding, fibroblast growth factor receptor 2 (FGFR2) activation causes angiogenesis, migration, and metastasis in diverse cancers, such as breast cancer (Wu et al., 2015), epithelial ovarian cancer (Li et al., 2018), and melanoma (Tsimafeyeu et al., 2016). Basic fibroblast growth factor (bFGF, also called FGF2) stimulation of FGFR2 results in Ca^{2+} channel-dependent upregulation of VEGF secretion in retinal pigment epithelial (RPE) cells (Rosenthal et al., 2005). Therefore, the detailed mechanisms by which brivanib affects the phosphorylation of VEGFR1 and FGFR2 during CNV formation need further exploration.

Receptor tyrosine kinases (RTKs) are transmembrane glycoproteins that play fundamental roles in intracellular tyrosine phosphorylation and intracellular signaling related to processes including cell proliferation, migration, differentiation, and apoptosis (Lemmon & Schlessinger, 2010). In addition, RTKs are involved in multiple pathological conditions, such as cancer and metabolic and autoimmune disorders (Gschwind, Fischer, & Ullrich, 2004; Hoch et al., 2001; Sourdon et al., 2017). Thus far, targeted RTK inhibitors have been successfully utilized in the treatment of multiple cancer types (Gaumann et al., 2016). Most of these inhibitors are multitargeting drugs that target VEGFR and FGFR, such as brivanib, lenvatinib, and dovitinib (Ferguson & Gray, 2018). In our study, brivanib inhibited the phosphorylation of VEGFR2 and FGFR1, hence blocking downstream signaling pathways and ultimately reducing CNV leakage, area, and

formation. Lenvatinib, an oral inhibitor of VEGFR1–3, FGFR1–4, platelet-derived growth factor receptor α, RET (the product of the c-ret proto-oncogene), and KIT (the product of the c-kit proto-oncogene), is associated with significant improvements in progression-free survival and response rates among patients with iodine-131-refractory thyroid cancer (Schlumberger et al., 2015). Lenvatinib rapidly penetrates the blood–retina barrier (BRB) to reach the retina after oral administration, inhibiting laser-induced CNV with high efficacy in mice (Wei et al., 2018). Dovitinib shows modest antitumor activity with manageable toxicity in men with metastatic castration-resistant prostate cancer (mCRPC). In particular, chemo-naïve mCRPC patients benefit from dovitinib (Choi et al., 2018). These data indicate a bright future for RTK inhibitors in the treatment of nAMD.

Diabetic retinopathy (DR) is characterized by leukostasis, hyperpermeability, and capillary degeneration followed by pathological retinal neovascularization (Zhang, Liu, Al-Shabrawey, Caldwell, & Caldwell, 2011). These vascular changes are also associated with different growth factors, such as angiopoietin, VEGF, and FGF (Cross & Claesson-Welsh, 2001; Grant et al., 2004). Previous studies have indicated that VEGFR and FGFR play vital roles in the pathogenesis of DR (Hueber, Wiedemann, Esser, & Heimann, 1996; Mei et al., 2018). In a mouse model of ischemia-induced retinopathy, a single intravitreal injection of 40 μM PTK/ZK was found to be capable of significantly reducing angioproliferative retinopathy (Maier et al., 2005). Therefore, whether brivanib can be used for the treatment of DR warrants an in-depth study.

In our study, we used two drug delivery methods, intravitreal injection and oral gavage, to investigate the effects and mechanisms of brivanib in laser-induced CNV in mice. The data showed that both methods could reduce CNV leakage and area, suggesting that brivanib had the capability of penetrating the BRB. However, we did not perform liquid chromatography-tandem mass spectrometry (LC/MS/MS) to measure the $T_{1/2}$ (half-time) of brivanib in the mouse retina following oral gavage. In previous studies, brivanib has usually been orally administered to mice (Huynh et al., 2008; Nakamura et al., 2014; Tovar et al., 2017). In this study, we also administered brivanib via intravitreal injection, one of the most commonly performed surgical procedures in ophthalmology (Falavarjani & Nguyen, 2013). Among the various complications of intravitreal injection, endophthalmitis can be a sight hazard (Shah et al., 2011). In the future, we will try to determine the optimal administration route for brivanib.

FIGURE 5 Brivanib oral gavage reduces CNV leakage and area. (a) Schematic diagram of the experimental procedure. The mice (CNV Day 14 group) were treated with the laser on Day 0. Starting on Day 3, 100 or 200 mg/kg/day brivanib was orally gavaged until Day 7. On Day 14, the eye tissues of the mice were collected and analyzed. (b) FFA and (c) ICGA of CNV lesions were performed in the normal, CNV Day 14, 100 mg/kg/day brivanib and 200 mg/kg/day brivanib groups. (d) The mouse CNV lesion areas were assessed Day 14 after CNV induction by staining of choroidal flat mounts with phalloidin and IB4. Scale bar = 100 μm. (e) Fluorescein leakage in CNV lesions was graded Day 14 after CNV in the control (n = 32 lesions), 200 mg/kg/day brivanib (n = 30 lesions), and 300 mg/kg/day brivanib (n = 32 lesions) groups. n = 5/group. (f) The mean intensity values representing CNV leakage were assessed by FFA and quantified. **p < .01 versus the Day 14 group. (g) Quantification of the CNV area. **p < .01 versus the CNV Day 14 group. Mean plasma (H) and retinal/choroidal/scleral (I) concentration–time profiles of brivanib in mice after oral gavage of [^{14}C] brivanib alaninate. CNV: choroidal neovascularization; FFA: fundus fluorescein angiography; ICGA: indocyanine green angiography [Color figure can be viewed at wileyonlinelibrary.com]
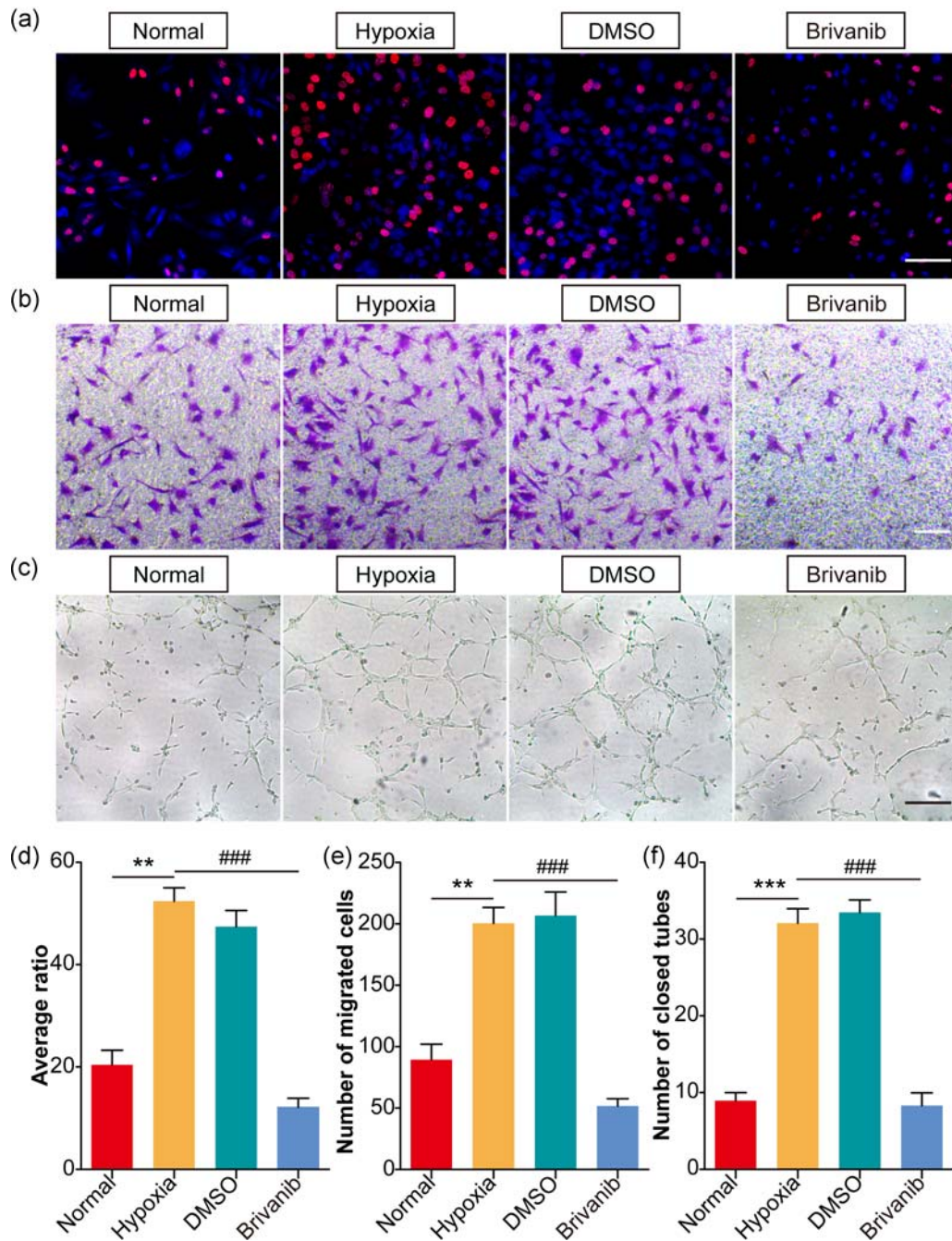
FIGURE 6 Brivanib inhibits the proliferation, migration, and tube formation of b-End3 cells in vitro. B-End3 cells were randomly divided into four groups: The normal, hypoxia (0.4 mM DMOG treatment for 6 hr), hypoxia plus DMSO (0.5% DMSO treatment for 6 hr), and hypoxia plus brivanib (10 μM brivanib treatment for 6 hr) groups. (a) An EdU assay was performed to measure the proliferation capability of b-End3 cells. (d) The EdU-positive cell ratio was analyzed. **$p < .01$ versus the normal group. ***$p < .005$ versus the hypoxia group. (b) A transwell assay was performed to detect the migration capability of b-End3 cells. (e) The number of migrated cells was analyzed. **$p < .01$ versus the normal group. ***$p < .005$ versus the hypoxia group. (c) A tube formation assay was performed. (f) The number of closed tubes was analyzed. ***$p < .005$ versus the normal group. ###$p < .005$ versus the hypoxia group. Scale bar = 100 μm. $n = 5$/group. DMSO: dimethyl sulfoxide; EdU: 5-ethynyl-20-deoxyuridine [Color figure can be viewed at wileyonlinelibrary.com]

In summary, brivanib inhibited zebrafish embryonic angiogenesis without impairing neurodevelopment. In a mouse CNV model, brivanib intravitreal injection blocked the phosphorylation of FGFR1 and VEGFR2 and reduced CNV leakage, area, and formation without causing intraocular toxicity. Moreover, brivanib oral gavage reduced CNV leakage and area. Accordingly, brivanib maintained high concentrations (above 14,000 ng/ml) in retinal/choroidal/scleral tissues following intravitreal injection. Similarly, brivanib remained at high concentrations (10,000 ng/ml) in retinal/choroidal/scleral tissues following oral gavage. Finally, in vitro cell experiments

demonstrated that brivanib inhibited the proliferation, migration and tube formation of microvascular endothelial cells. However, there are still several shortcomings of our study, including a lack of analysis of the metabolism of brivanib in the mouse body, a lack of analysis of other VEGFRs and FGFRs, and a lack of determination of the detailed mechanisms by which brivanib reduces CNV formation. These limitations will provide direction for our future research.

CONFLICT OF INTEREST

The authors declare that there is no conflict of interest.

AUTHOR CONTRIBUTIONS

Guarantors of the integrity of the entire study: A. S. and D. D.; Study conception/design, data acquisition, and data analysis/interpretation: all authors; Manuscript drafting and manuscript revision for important intellectual content: all authors; Manuscript final version approval: all authors; Answering/appropriately resolving any future questions related to the work: all authors; Literature research: L. L., M. Z., X. L., A. S., and D. D.; Statistical analysis: W. W., B. Q., J. G., Y. T., J. C., D. L., Y. S., A. S., and D. D.

ORCID

Aimin Sang (iD) http://orcid.org/0y000-0002-9669-403X

REFERENCES

Aiello, L. P., Pierce, E. A., Foley, E. D., Takagi, H., Chen, H., Riddle, L., … Smith, L. E. (1995). Suppression of retinal neovascularization in vivo by inhibition of vascular endothelial growth factor (VEGF) using soluble VEGF-receptor chimeric proteins. *Proceedings of the National Academy of Sciences of the United States of America, 92*(23), 10457–10461.

Amadio, M., Govoni, S., & Pascale, A. (2016). Targeting VEGF in eye neovascularization: What's new?: A comprehensive review on current therapies and oligonucleotide-based interventions under development. *Pharmacological Research, 103*, 253–269. https://doi.org/10.1016/j.phrs.2015.11.027

Andreoli, C. M., & Miller, J. W. (2007). Anti-vascular endothelial growth factor therapy for ocular neovascular disease. *Current Opinion in Ophthalmology, 18*(6), 502–508. https://doi.org/10.1097/ICU.0b013e3282f0ca54

Ayers, M., Fargnoli, J., Lewin, A., Wu, Q., & Platero, J. S. (2007). Discovery and validation of biomarkers that respond to treatment with brivanib

alaninate, a small-molecule VEGFR-2/FGFR-1 antagonist. *Cancer Research, 67*(14), 6899–6906. https://doi.org/10.1158/0008-5472.CAN-06-4555

Ba-Sang, D. Z., Long, Z. W., Teng, H., Zhao, X. P., Qiu, J., & Li, M. S. (2016). A network meta-analysis on the efficacy of sixteen targeted drugs in combination with chemotherapy for treatment of advanced/metastatic colorectal cancer. *Oncotarget, 7*(51), 84468–84479. https://doi.org/10.18632/oncotarget.12994

Bergers, G., & Hanahan, D. (2008). Modes of resistance to anti-angiogenic therapy. *Nature Reviews Cancer, 8*(8), 592–603. https://doi.org/10.1038/nrc2442

Bhide, R. S., Lombardo, L. J., Hunt, J. T., Cai, Z. W., Barrish, J. C., Galbraith, S., & Fargnoli, J. (2010). The antiangiogenic activity in xenograft models of brivanib, a dual inhibitor of vascular endothelial growth factor receptor-2 and fibroblast growth factor receptor-1 kinases. *Molecular Cancer Therapeutics, 9*(2), 369–378. https://doi.org/10.1158/1535-7163.MCT-09-0472

Cao, R., Ji, H., Feng, N., Zhang, Y., Yang, X., Andersson, P., & Cao, Y. (2012). Collaborative interplay between FGF-2 and VEGF-C promotes lymphangiogenesis and metastasis. *Proceedings of the National Academy of Sciences of the United States of America, 109*(39), 15894–15899. https://doi.org/10.1073/pnas.1208324109

Chan, J. K., Deng, W., Higgins, R. V., Tewari, K. S., Bonebrake, A. J., Hicks, M., & Aghajanian, C. (2017). A phase II evaluation of brivanib in the treatment of persistent or recurrent carcinoma of the cervix: An NRG Oncology/Gynecologic Oncology Group study. *Gynecologic Oncology, 146*(3), 554–559. https://doi.org/10.1016/j.ygyno.2017.05.033

Chiodelli, P., Rezzola, S., Urbinati, C., Federici Signori, F., Monti, E., Ronca, R., & Rusnati, M. (2017). Contribution of vascular endothelial growth factor receptor-2 sialylation to the process of angiogenesis. *Oncogene, 36*(47), 6531–6541. https://doi.org/10.1038/onc.2017.243

Choi, Y. J., Kim, H. S., Park, S. H., Kim, B. S., Kim, K. H., Lee, H. J., & Park, K. H. (2018). Phase II study of dovitinib in patients with castration-resistant prostate cancer (KCSG-GU11-05). *Cancer Research and Treatment: Official Journal of Korean Cancer Association, 50*(4), 1252–1259. https://doi.org/10.4143/crt.2017.438

Crespo-Garcia, S., Corkhill, C., Roubeix, C., Davids, A. M., Kociok, N., Strauss, O., & Reichhart, N. (2017). Inhibition of placenta growth factor reduces subretinal mononuclear phagocyte accumulation in choroidal neovascularization. *Investigative Ophthalmology and Visual Science, 58*(12), 4997–5006. https://doi.org/10.1167/iovs.16-21283

Cross, M. J., & Claesson-Welsh, L. (2001). FGF and VEGF function in angiogenesis: Signalling pathways, biological responses and therapeutic inhibition. *Trends in Pharmacological Sciences, 22*(4), 201–207.

Cucchetti, A., Piscaglia, F., Pinna, A. D., Djulbegovic, B., Mazzotti, F., & Bolondi, L. (2017). Efficacy and safety of systemic therapies for advanced hepatocellular carcinoma: A network meta-analysis of phase III trials. *Liver Cancer, 6*(4), 337–348. https://doi.org/10.1159/000481314

Dewan, A., Liu, M., Hartman, S., Zhang, S. S., Liu, D. T., Zhao, C., & Hoh, J. (2006). HTRA1 promoter polymorphism in wet age-related macular degeneration. *Science, 314*(5801), 989–992. https://doi.org/10.1126/science.1133807

Diaz-Padilla, I., & Siu, L. L. (2011). Brivanib alaninate for cancer. *Expert Opinion on Investigational Drugs, 20*(4), 577–586. https://doi.org/10.1517/13543784.2011.565329

Falavarjani, K. G., & Nguyen, Q. D. (2013). Adverse events and complications associated with intravitreal injection of anti-VEGF agents: A review of literature. *Eye (Lond), 27*(7), 787–794. https://doi.org/10.1038/eye.2013.107

Feng, S., Zhou, L., Nice, E. C., & Huang, C. (2015). Fibroblast growth factor receptors: Multifactorial-contributors to tumor initiation and progression. *Histology and Histopathology, 30*(1), 13–31. https://doi.org/10.14670/HH-30.13

Ferguson, F. M., & Gray, N. S. (2018). Kinase inhibitors: The road ahead. *Nature Reviews. Drug Discovery*, 17(5), 353–377. https://doi.org/10.1038/nrd.2018.21

Gaumann, A. K., Kiefer, F., Alfer, J., Lang, S. A., Geissler, E. K., & Breier, G. (2016). Receptor tyrosine kinase inhibitors: Are they real tumor killers? *International Journal of Cancer*, 138(3), 540–554. https://doi.org/10.1002/ijc.29499

Gouaze-Andersson, V., Delmas, C., Taurand, M., Martinez-Gala, J., Evrard, S., Mazoyer, S., & Cohen-Jonathan-Moyal, E. (2016). FGFR1 induces glioblastoma radioresistance through the PLCgamma/Hif1alpha pathway. *Cancer Research*, 76(10), 3036–3044. https://doi.org/10.1158/0008-5472.CAN-15-2058

Grant, M. B., Afzal, A., Spoerri, P., Pan, H., Shaw, L. C., & Mames, R. N. (2004). The role of growth factors in the pathogenesis of diabetic retinopathy. *Expert Opinion on Investigational Drugs*, 13(10), 1275–1293. https://doi.org/10.1517/13543784.13.10.1275

Gschwind, A., Fischer, O. M., & Ullrich, A. (2004). The discovery of receptor tyrosine kinases: Targets for cancer therapy. *Nature Reviews Cancer*, 4(5), 361–370. https://doi.org/10.1038/nrc1360

Hoch, W., McConville, J., Helms, S., Newsom-Davis, J., Melms, A., & Vincent, A. (2001). Auto-antibodies to the receptor tyrosine kinase MuSK in patients with myasthenia gravis without acetylcholine receptor antibodies. *Nature Medicine (New York, NY, United States)*, 7(3), 365–368. https://doi.org/10.1038/85520

Hueber, A., Wiedemann, P., Esser, P., & Heimann, K. (1996). Basic fibroblast growth factor mRNA, bFGF peptide and FGF receptor in epiretinal membranes of intraocular proliferative disorders (PVR and PDR). *International Ophthalmology*, 20(6), 345–350.

Huynh, H., Ngo, V. C., Fargnoli, J., Ayers, M., Soo, K. C., Koong, H. N., & Tran, E. (2008). Brivanib alaninate, a dual inhibitor of vascular endothelial growth factor receptor and fibroblast growth factor receptor tyrosine kinases, induces growth inhibition in mouse models of human hepatocellular carcinoma. *Clinical Cancer Research*, 14(19), 6146–6153. https://doi.org/10.1158/1078-0432.CCR-08-0509

Izumi-Nagai, K., Nagai, N., Ohgami, K., Satofuka, S., Ozawa, Y., Tsubota, K., & Ishida, S. (2008). Inhibition of choroidal neovascularization with an anti-inflammatory carotenoid astaxanthin. *Investigative Ophthalmology and Visual Science*, 49(4), 1679–1685. https://doi.org/10.1167/iovs.07-1426

Johnson, P. J., Qin, S., Park, J. W., Poon, R. T., Raoul, J. L., Philip, P. A., & Cheng, A. L. (2013). Brivanib versus sorafenib as first-line therapy in patients with unresectable, advanced hepatocellular carcinoma: Results from the randomized phase III BRISK-FL study. *Journal of Clinical Oncology*, 31(28), 3517–3524. https://doi.org/10.1200/JCO.2012.48.4410

Kudo, M., Han, G., Finn, R. S., Poon, R. T., Blanc, J. F., Yan, L., & Wang, J. H. (2014). Brivanib as adjuvant therapy to transarterial chemoembolization in patients with hepatocellular carcinoma: A randomized phase III trial. *Hepatology*, 60(5), 1697–1707. https://doi.org/10.1002/hep.27290

Lemmon, M. A., & Schlessinger, J. (2010). Cell signaling by receptor tyrosine kinases. *Cell*, 141(7), 1117–1134. https://doi.org/10.1016/j.cell.2010.06.011

Li, M., Qian, Z., Ma, X., Lin, X., You, Y., Li, Y., & Jiang, H. (2018). MiR-628-5p decreases the tumorigenicity of epithelial ovarian cancer cells by targeting at FGFR2. *Biochemical and Biophysical Research Communications*, 495(2), 2085–2091. https://doi.org/10.1016/j.bbrc.2017.12.049

Lim, L. S., Mitchell, P., Seddon, J. M., Holz, F. G., & Wong, T. Y. (2012). Age-related macular degeneration. *Lancet*, 379(9827), 1728–1738. https://doi.org/10.1016/S0140-6736(12)60282-7

Maier, P., Unsoeld, A. S., Junker, B., Martin, G., Drevs, J., Hansen, L. L., & Agostini, H. T. (2005). Intravitreal injection of specific receptor tyrosine kinase inhibitor PTK787/ZK222 584 improves ischemia-induced retinopathy in mice. *Graefes Archive for Clinical and Experimental Ophthalmology*, 243(6), 593–600. https://doi.org/10.1007/s00417-004-1021-9

Matsushima, M., Ogata, N., Takada, Y., Tobe, T., Yamada, H., Takahashi, K., & Uyama, M. (1996). FGF receptor 1 expression in experimental choroidal neovascularization. *Japanese Journal of Ophthalmology*, 40(3), 329–338.

Mei, X., Zhou, L., Zhang, T., Lu, B., Sheng, Y., & Ji, L. (2018). Chlorogenic acid attenuates diabetic retinopathy by reducing VEGF expression and inhibiting VEGF-mediated retinal neoangiogenesis. *Vascular Pharmacology*, 101, 29–37. https://doi.org/10.1016/j.vph.2017.11.002

Munk, M. R., Ruckert, R., Zinkernagel, M., Ebneter, A., & Wolf, S. (2016). The role of anti-VEGF agents in myopic choroidal neovascularization: Current standards and future outlook. *Expert Opinion on Biological Therapy*, 16(4), 477–487. https://doi.org/10.1517/14712598.2016.1132696

Nakamura, I., Zakharia, K., Banini, B. A., Mikhail, D. S., Kim, T. H., Yang, J. D., & Roberts, L. R. (2014). Brivanib attenuates hepatic fibrosis in vivo and stellate cell activation in vitro by inhibition of FGF, VEGF and PDGF signaling. *PLOS One*, 9(4), e92273. https://doi.org/10.1371/journal.pone.0092273

Ng, D. S. C., Lai, T. Y. Y., Cheung, C. M. G., & Ohno-Matsui, K. (2017). Anti-vascular endothelial growth factor therapy for myopic choroidal neovascularization. *Asia-Pacific Journal of Ophthalmology (Philadelphia, Pa)*, 6(6), 554–560. https://doi.org/10.22608/APO.2017308

Oladipupo, S. S., Smith, C., Santeford, A., Park, C., Sene, A., Wiley, L. A., & Ornitz, D. M. (2014). Endothelial cell FGF signaling is required for injury response but not for vascular homeostasis. *Proceedings of the National Academy of Sciences of the United States of America*, 111(37), 13379–13384. https://doi.org/10.1073/pnas.1324235111

Papa, A., Zaccarelli, E., Caruso, D., Vici, P., Benedetti Panici, P., & Tomao, F. (2016). Targeting angiogenesis in endometrial cancer - new agents for tailored treatments. *Expert Opinion on Investigational Drugs*, 25(1), 31–49. https://doi.org/10.1517/13543784.2016.1116517

Rosenthal, R., Malek, G., Salomon, N., Peill-Meininghaus, M., Coeppicus, L., Wohlleben, H., & Strauss, O. (2005). The fibroblast growth factor receptors, FGFR-1 and FGFR-2, mediate two independent signalling pathways in human retinal pigment epithelial cells. *Biochemical and Biophysical Research Communications*, 337(1), 241–247. https://doi.org/10.1016/j.bbrc.2005.09.028

Ryu, J. K., Cho, T., Choi, H. B., Wang, Y. T., & McLarnon, J. G. (2009). Microglial VEGF receptor response is an integral chemotactic component in Alzheimer's disease pathology. *Journal of Neuroscience*, 29(1), 3–13. https://doi.org/10.1523/JNEUROSCI.2888-08.2009

Schlumberger, M., Tahara, M., Wirth, L. J., Robinson, B., Brose, M. S., Elisei, R., & Sherman, S. I. (2015). Lenvatinib versus placebo in radioiodine-refractory thyroid cancer. *New England Journal of Medicine*, 372(7), 621–630. https://doi.org/10.1056/NEJMoa1406470

Shah, C. P., Garg, S. J., Vander, J. F., Brown, G. C., Kaiser, R. S., & Haller, J. A., Post-Injection Endophthalmitis Study, T. (2011). Outcomes and risk factors associated with endophthalmitis after intravitreal injection of anti-vascular endothelial growth factor agents. *Ophthalmology*, 118(10), 2028–2034. https://doi.org/10.1016/j.ophtha.2011.02.034

Sourdon, J., Lager, F., Viel, T., Balvay, D., Moorhouse, R., Bennana, E., & Tavitian, B. (2017). Cardiac metabolic deregulation induced by the tyrosine kinase receptor inhibitor Sunitinib is rescued by endothelin receptor antagonism. *Theranostics*, 7(11), 2757–2774. https://doi.org/10.7150/thno.19551

Sun, H. J., Cai, W. W., Gong, L. L., Wang, X., Zhu, X. X., Wan, M. Y., & Qiu, L. Y. (2017). FGF-2-mediated FGFR1 signaling in human microvascular endothelial cells is activated by vaccarin to promote angiogenesis. *Biomedicine and Pharmacotherapy*, 95, 144–152. https://doi.org/10.1016/j.biopha.2017.08.059

Sun, W., & Cabrera, R. (2018). Systemic treatment of patients with advanced, unresectable hepatocellular carcinoma: Emergence of

therapies. *Journal of Gastrointestinal Cancer*, 49(2), 107–115. https://doi.org/10.1007/s12029-018-0065-8

Tovar, V., Cornella, H., Moeini, A., Vidal, S., Hoshida, Y., Sia, D., & Llovet, J. M. (2017). Tumour initiating cells and IGF/FGF signalling contribute to sorafenib resistance in hepatocellular carcinoma. *Gut*, 66(3), 530–540. https://doi.org/10.1136/gutjnl-2015-309501

Tsimafeyeu, I., Ludes-Meyers, J., Stepanova, E., Daeyaert, F., Khochenkov, D., Joose, J. B., & Tjulandin, S. (2016). Targeting FGFR2 with alofanib (RPT835) shows potent activity in tumour models. *European Journal of Cancer*, 61, 20–28. https://doi.org/10.1016/j.ejca.2016.03.068

Van deVeire, S., Stalmans, I., Heindryckx, F., Oura, H., Tijeras-Raballand, A., Schmidt, T., & Carmeliet, P. (2010). Further pharmacological and genetic evidence for the efficacy of PlGF inhibition in cancer and eye disease. *Cell*, 141(1), 178–190. https://doi.org/10.1016/j.cell.2010.02.039

Wei, X., Zhang, T., Yao, Y., Zeng, S., Li, M., Xiang, H., & Yang, J. (2018). Efficacy of Lenvatinib, a multitargeted tyrosine kinase inhibitor, on laser-induced CNV mouse model of neovascular AMD. *Experimental Eye Research*, 168, 2–11. https://doi.org/10.1016/j.exer.2017.12.009

Williams, R. L., Risau, W., Zerwes, H. G., Drexler, H., Aguzzi, A., & Wagner, E. F. (1989). Endothelioma cells expressing the polyoma middle T oncogene induce hemangiomas by host cell recruitment. *Cell*, 57(6), 1053–1063.

Wu, X. Y., Xu, H., Wu, Z. F., Chen, C., Liu, J. Y., Wu, G. N., & Shen, L. (2015). Formononetin, a novel FGFR2 inhibitor, potently inhibits angiogenesis and tumor growth in preclinical models. *Oncotarget*, 6(42), 44563–44578. https://doi.org/10.18632/oncotarget.6310

Yu, H. G., Liu, X., Kiss, S., Connolly, E., Gragoudas, E. S., Michaud, N. A., & Kim, I. K. (2008). Increased choroidal neovascularization following laser induction in mice lacking lysyl oxidase-like 1. *Investigative Ophthalmology and Visual Science*, 49(6), 2599–2605. https://doi.org/10.1167/iovs.07-1508

Yu, X., Qi, Y., Zhao, T., Fang, J., Liu, X., Xu, T., & Dai, X. (2018). NGF increases FGF2 expression and promotes endothelial cell migration and tube formation through PI3K/Akt and ERK/MAPK pathways in human chondrocytes. *Osteoarthritis and Cartilage*, 27, 526–534. https://doi.org/10.1016/j.joca.2018.12.007

Zhang, W., Liu, H., Al-Shabrawey, M., Caldwell, R. W., & Caldwell, R. B. (2011). Inflammation and diabetic retinal microvascular complications. *Journal of Cardiovascular Disease Research*, 2(2), 96–103. https://doi.org/10.4103/0975-3583.83035

Zhang, Y., Han, Q., Ru, Y., Bo, Q., & Wei, R. H. (2015). Anti-VEGF treatment for myopic choroid neovascularization: From molecular characterization to update on clinical application. *Drug Design, Development and Therapy*, 9, 3413–3421. https://doi.org/10.2147/DDDT.S87920

Zubilewicz, A., Hecquet, C., Jeanny, J. C., Soubrane, G., Courtois, Y., & Mascarelli, F. (2001). Two distinct signalling pathways are involved in FGF2-stimulated proliferation of choriocapillary endothelial cells: A comparative study with VEGF. *Oncogene*, 20(12), 1403–1413. https://doi.org/10.1038/sj.onc.1204231